Regulatory roles of fibronectin and integrin α5 in reorganization of the actin cytoskeleton and completion of adipogenesis

Megumi Uetaki[a,†], Nobuyuki Onishi[a], Yoshinao Oki[b], Takatsune Shimizu[c], Eiji Sugihara[d,e], Oltea Sampetrean[a], Takashi Watanabe[e], Hisano Yanagi[f], Kiyoshi Suda[g], Hiroya Fujii[h], Koichiro Kano[b], Hideyuki Saya[a,e,†], and Hiroyuki Nobusue[a,e,†,*]

[a]Division of Gene Regulation, Institute for Advanced Medical Research, Keio University School of Medicine, Tokyo, Japan; [b]Laboratory of Cell and Tissue Biology, College of Bioresource Sciences, Nihon University, Fujisawa, Japan; [c]Department of Pathophysiology, School of Pharmacy and Pharmaceutical Sciences, Hoshi University, Tokyo, Japan; [d]Open Facility Center, and [e]Division of Gene Regulation, Cancer Center, Research Promotion Headquarters, Fujita Health University, Toyoake, Japan; [f]Department of Medical Oncology, Fujita Health University School of Medicine, Toyoake, Japan; [g]JSR—Keio University Medical and Chemical Innovation Center (JKiC), JSR Corporation, Tokyo, Japan; [h]Medical & Biological Laboratories Co., Ltd., Tokyo, Japan

ABSTRACT Cellular differentiation is characterized by changes in cell morphology that are largely determined by actin dynamics. We previously showed that depolymerization of the actin cytoskeleton triggers the differentiation of preadipocytes into mature adipocytes as a result of inhibition of the transcriptional coactivator activity of megakaryoblastic leukemia 1 (MKL1). The extracellular matrix (ECM) influences cell morphology via interaction with integrins, and reorganization of the ECM is associated with cell differentiation. Here we show that interaction between actin dynamics and ECM rearrangement plays a key role in adipocyte differentiation. We found that depolymerization of the actin cytoskeleton precedes disruption and degradation of fibrillar fibronectin (FN) structures at the cell surface after the induction of adipogenesis in cultured preadipocytes. A FN matrix suppressed both reorganization of the actin cytoskeleton into the pattern characteristic of adipocytes and terminal adipocyte differentiation, and these inhibitory effects were overcome by knockdown of integrin α5 (ITGα5). Peroxisome proliferator–activated receptor γ was required for down-regulation of FN during adipocyte differentiation, and MKL1 was necessary for the expression of ITGα5. Our findings suggest that cell-autonomous down-regulation of FN-ITGα5 interaction contributes to reorganization of the actin cytoskeleton and completion of adipocyte differentiation.

INTRODUCTION

The extracellular matrix (ECM) is composed predominantly of two types of macromolecules: fibrous proteins, including collagens and elastin, and glycoproteins, including fibronectin (FN), proteoglycans, and laminin (Mouw *et al.*, 2014; Moreira *et al.*, 2020). Integrins are cell surface receptors for ECM components and transmit signals from the outside of the cell to the inside. They regulate reorganization of the actin cytoskeleton in response to ECM attachment, with such cell–matrix interaction having important roles in the control of various cellular processes including proliferation, differentiation, survival, and morphogenesis (Desgrosellier and Cheresh, 2010; Bonnans *et al.*, 2014). Individual ECM components have been shown to influence the differentiation of embryonic stem cells and various tissue stem cells in culture (Ma *et al.*, 2008; Gattazzo *et al.*, 2014; Hoshiba *et al.*, 2016). In addition, elasticity of the ECM has been found to determine cell fate and differentiation, with mesenchymal stem cells differentiating into osteoblasts or adipocytes when seeded on a rigid or soft ECM, respectively (Engler *et al.*, 2006; Guilak *et al.*, 2009; Ivanovska *et al.*, 2015). Mechanical cues present in the ECM are thus thought to provide signals that determine cell fate and differentiation.

Cells form a specialized microenvironment for their growth and differentiation by synthesizing and secreting specific ECM proteins (Kwon *et al.*, 2013; Blache *et al.*, 2020). During adipogenesis, ECM remodeling is associated with important events of the differentiation process. The FN-rich stromal matrix of preadipocytes is thus converted to the laminin-rich basement membrane of adipocytes (Lilla *et al.*, 2002; Ojima *et al.*, 2016). A FN matrix has been shown to inhibit adipocyte differentiation by preventing the associated cytoskeletal and morphological changes (Spiegelman and Ginty, 1983; Wang *et al.*, 2010). Remodeling of the actin cytoskeleton is a hallmark of adipocyte differentiation and is characterized by the conversion of filamentous (F-) actin from stress fibers and lamellipodia to cortical actin structures (Smas and Sul, 1995; Cristancho and Lazar, 2011).

We have previously shown that depolymerization of actin stress fibers triggers the expression of peroxisome proliferator–activated receptor γ (PPARγ), a master transcriptional regulator of adipogenesis (Rosen and MacDougald, 2006; Cristancho and Lazar, 2011), and drives terminal adipocyte differentiation in several adipogenic progenitor cells (Nobusue *et al.*, 2014; Takahashi *et al.*, 2019). In addition, we found that reorganization of the actin cytoskeleton from depolymerized actin to the pattern characteristic of adipocytes is essential for completion of adipocyte differentiation (Kunitomi *et al.*, 2020). The interrelations and cross-talk among such actin cytoskeletal dynamics, reorganization of the ECM, and the PPARγ-mediated adipocyte differentiation program have remained unclear, however.

We have now examined the interaction between actin dynamics and ECM remodeling with regard to the regulation of adipocyte differentiation. We found that a FN matrix suppresses both reorganization of the actin cytoskeleton from depolymerized actin to the pattern characteristic of adipocytes and the completion of adipogenesis, and that these inhibitory effects were overcome by knockdown of integrin α5 (ITGα5), a subunit of the FN receptor. Furthermore, ITGα5 expression was shown to be regulated directly by the interaction between actin dynamics and the transcriptional coactivator MKL1 (megakaryoblastic leukemia 1). Our results have clarified the relevance and mechanism of the ECM conversion that occurs during adipose differentiation induced by depolymerization of the actin cytoskeleton.

RESULTS

PPARγ regulates reorganization of the actin cytoskeleton through down-regulation of fibronectin during adipogenesis

We have previously established a preadipocyte cell line derived from mouse dedifferentiated fat (DFAT) cells that possesses a higher potential to differentiate into adipocytes than the embryonic mouse 3T3-L1 preadipocyte cell line (Nobusue *et al.*, 2008). We analyzed the expression patterns of preadipocyte- and adipocyte-selective genes in DFAT, 3T3-L1, and the embryonic mouse C3H10T1/2 mesenchymal stem cell line using microarray data sets obtained from GEO. Compared with 3T3-L1 and C3H10T1/2 cells, DFAT cells were found to express preadipocyte-selective genes (*Dlk1* and *Pdgfra*) at a low level but adipocyte-selective genes (*Pparg* and *Cebpa*) at a high level (Supplemental Figure S1A), implying that DFAT cells possess a sort of memory of adult mature adipocytes from which they are derived and might be a later stage of the adipocyte differentiation program than 3T3-L1 cells. Furthermore, DFAT cells do not undergo spontaneous adipogenesis, unlike 3T3-L1 cells, as we previously described (Yagi *et al.*, 2004; Nobusue *et al.*, 2008). We also found that DFAT cells did not undergo cell division after the induction of adipocytic differentiation, unlike 3T3-L1 cells (Supplemental Figure S1B). Our findings show that the DFAT cell line is a useful model for investigating the morphological dynamics of individual cells after exposure to the inducers of adipocyte differentiation. We first examined changes in the ECM during adipogenesis with the use of these DFAT cells. Before induction of adipogenesis, both *Fn1* mRNA and FN protein were detected at a high level in DFAT cells, which manifested a fibroblastic morphology with both well-developed actin stress fibers and fibrillar FN structures at the cell surface that appeared connected to the actin cytoskeleton (Figure 1, A and B). At 24 h after the induction of adipocytic differentiation, the cells exhibited a well-spread morphology associated with disruption of most stress fibers and the fibrillar FN structures (Figure 1B). The up-regulation of *Pparg* mRNA was evident at 48 h (Figure 1A), at which time the amounts of both *Fn1* mRNA and FN protein were markedly decreased, the FN matrix had disappeared, and the cells had adopted a rounded morphology with a corresponding architecture of the actin cytoskeleton (Figure 1, B and C). Adipocytes have a characteristic round morphology that allows for maximal lipid storage (Smas and Sul, 1995); we thus adopted cell roundness as the morphological criterion of an adipocyte-associated actin structure and measured roundness of the individual cells during adipogenesis using the images of the actin cytoskeleton. Furthermore, we examined the changes in the actin cytoskeleton and a FN matrix in DFAT and human preadipocyte (HPAd) cells cultured on soft ECM substrates mimicking the native matrix stiffness of adipose tissue (2 kPa; Discher *et al.*, 2009). Similarly to cells cultured on stiff glass or plastic substrates, both of those cells exhibited a decrease of FN, as well as reorganization into an adipocyte-associated actin structure after adipogenic induction (Figure 1, D and E; Supplemental Figure S2, A and B). These results thus suggested that the disruption of actin stress fibers precedes the disappearance of fibrillar FN structures, which is in turn followed by reorganization of the actin cytoskeleton into the pattern characteristic of adipocytes during adipocyte differentiation.

To test whether PPARγ contributes to down-regulation of *Fn1* expression during adipogenesis, we investigated the effects of PPARγ knockdown. We established DFAT cells that stably express a PPARγ short hairpin RNA (shRNA) and confirmed that they had lost adipogenic potential (Supplemental Figure S3, A and B). Whereas control cells expressing a luciferase shRNA (DFAT-shLuc) manifested a marked decrease in the abundance of *Fn1* mRNA and FN protein after exposure to inducers of adipocytic differentiation, cells
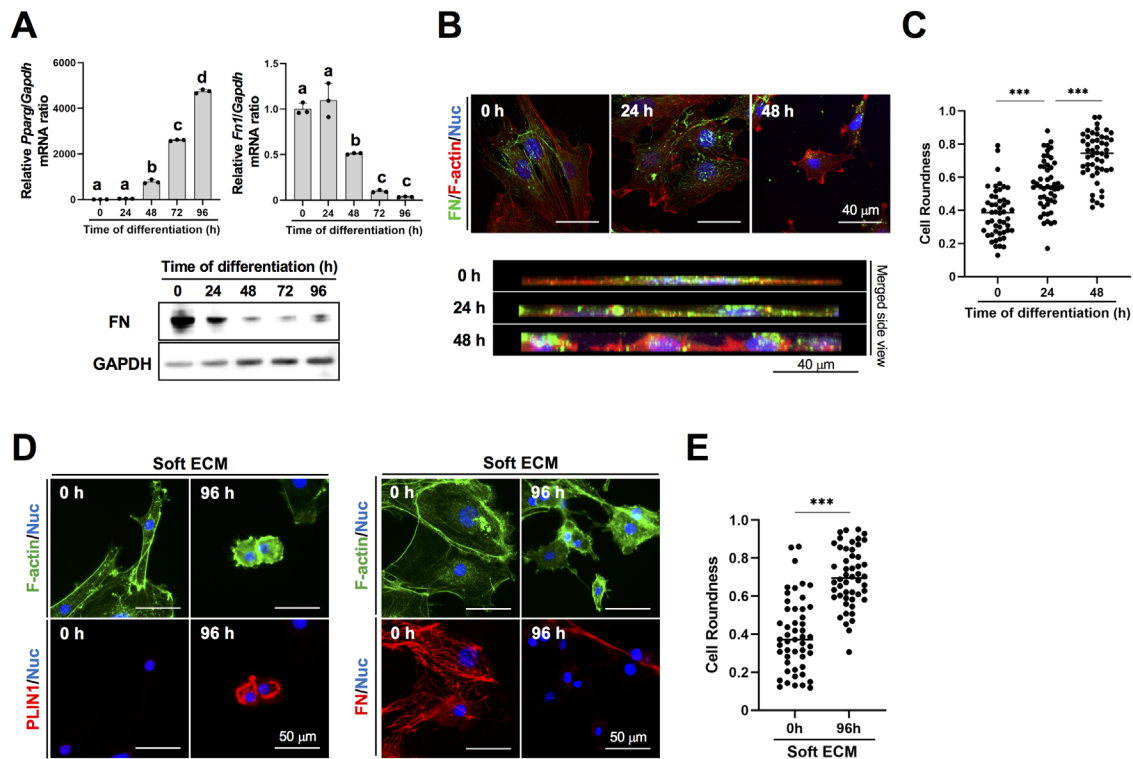
FIGURE 1: Down-regulation of FN and reorganization of the actin cytoskeleton during adipogenesis in DFAT cells. (A) RT and real-time PCR analysis of the relative abundance of *Pparg* and *Fn1* mRNAs (Upper) and immunoblot analysis of FN and glyceraldehyde-3-phosphate dehydrogenase (GAPDH, loading control; Lower) in DFAT cells exposed to inducers of adipocytic differentiation. [a–d]$p < 0.05$ Tukey's honest significant difference test. (B) Fluorescence microscopy of the actin cytoskeleton (stained with phalloidin) and of FN expression during adipogenesis in DFAT cells. Nuclei (Nuc) were stained with Hoechst 33342. Scale bars, 40 µm. (C) Cell roundness was measured in 50 individual cells shown as in B, with 1 indicating a perfect circle. (D) Fluorescence microscopy of the actin cytoskeleton (stained with phalloidin) and of perilipin 1 (PLIN1, marker of terminal adipocyte differentiation; Left) or of FN expression (Right) in DFAT cells cultured on a soft ECM (2 kPa) exposed to inducers of adipogenesis for 0 or 96 h. Nuclei (Nuc) were stained with Hoechst 33342. Scale bars, 50 µm. (E) Cell roundness was measured in 50 individual cells shown as in D, with 1 indicating a perfect circle. Quantitative data represent the mean ± s.d. from three independent experiments, A. ***$p < 0.001$ (Student's *t* test).

expressing the PPARγ shRNA (DFAT-shPPARγ) actually showed an increase (Figure 2A). Disruption of actin stress fibers and the fibrillar FN structures was apparent in both DFAT-shLuc and DFAT-shPPARγ cells at 24 h after the induction of adipogenesis (Figure 2B). However, subsequent reorganization of the actin cytoskeleton into the pattern characteristic of adipocytes occurred in DFAT-shLuc cells but not in DFAT-shPPARγ cells (Figure 2, B and C).

We next examined the effect of FN knockdown on reorganization of the actin cytoskeleton in DFAT-shPPARγ cells after exposure to inducers of adipocytic differentiation. Expression of FN at both the mRNA and protein levels in cells transfected with small interfering RNAs (siRNAs) specific for *Fn1* mRNA (si*Fn1*-#1 or si*Fn1*-#2) was greatly decreased from that in cells transfected with a control siRNA (si*Cont*) (Figure 2D). Knockdown of FN elicited the adoption of a rounded morphology with corresponding reorganization of the actin cytoskeleton in DFAT-shPPARγ cells exposed to inducers of adipocytic differentiation (Figure 2, E and F). On the other hand, depletion of FN did not influence the expression of adipogenic differentiation markers in these cells (Supplemental Figure S3C). Together, these findings suggested that PPARγ contributes to the down-regulation of FN during adipocyte differentiation, which in turn triggers reorganization of the actin cytoskeleton into the pattern characteristic of adipocytes.

A fibronectin matrix suppresses both reorganization of the actin cytoskeleton into the pattern characteristic of adipocytes and completion of adipogenesis

To investigate further the role of a FN matrix in reorganization of the actin cytoskeleton and adipocyte differentiation, we seeded DFAT cells on fibronectin-coated plates and exposed them to inducers of adipogenesis for 96 h. The FN substrate significantly suppressed the expression of adipogenic differentiation genes and the extent of lipid droplet accumulation in a concentration-dependent manner (Figure 3, A–C). Although depolymerization of the actin cytoskeleton was observed in DFAT cells cultured on a FN substrate in the presence of the adipogenic cocktail, its subsequent reorganization into the pattern typical of adipocytes was markedly impaired (Figure 3, C and D). In addition, FN coating also blocked the actin reorganization and the completion of adipogenesis in both 3T3-L1 and HPAd cells (Supplemental Figure S4). Furthermore, administration of FN to the culture medium also inhibited adipogenesis in DFAT cells (Supplemental Figure S5). We also found that depletion of FN accelerated their adipogenesis in DFAT cells exposed to inducers of adipocyte differentiation (Supplemental Figure S6). These data thus indicated that a FN matrix suppresses both reorganization of the actin cytoskeleton into the pattern characteristic of adipocytes and terminal adipocyte differentiation.
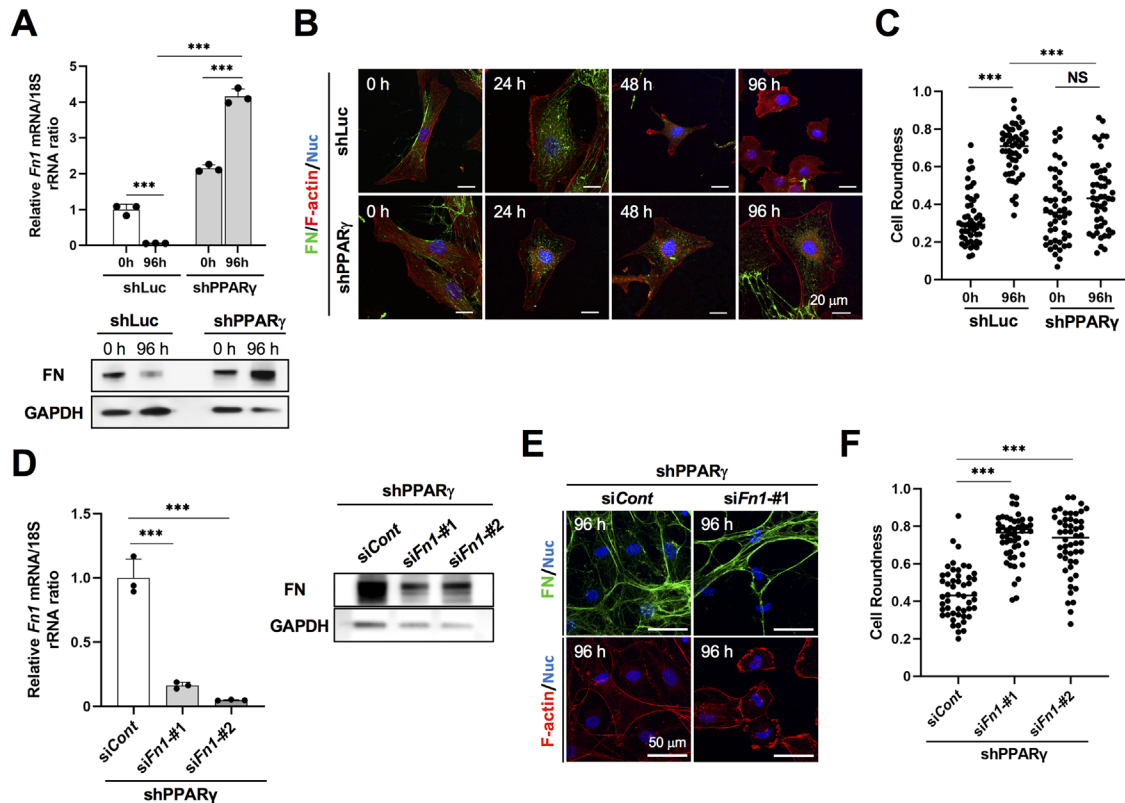
FIGURE 2: PPARγ contributes to reorganization of the actin cytoskeleton through down-regulation of FN during adipogenesis in DFAT cells. (A) Relative abundance of *Fn1* mRNA (Upper) and immunoblot analysis of FN (Lower) in DFAT cells stably expressing PPARγ (shPPARγ) or luciferase (shLuc, control) shRNAs exposed to inducers of adipogenesis for 0 or 96 h. (B) Fluorescence microscopy of the actin cytoskeleton and of FN expression in cells treated as in A. Nuclei (Nuc) were stained with Hoechst 33342. Scale bars, 20 µm. (C) Cell roundness was measured in 50 individual cells shown as in B, with 1 indicating a perfect circle. (D) Relative abundance of *Fn1* mRNA (left) and immunoblot analysis of FN (right) in DFAT cells stably expressing shPPARγ, transfected with *Fn1* (si*Fn1*-#1 or -#2) or control (si*Cont*) siRNAs, and exposed to inducers of adipogenesis for 96 h. (E) Fluorescence microscopy of the actin cytoskeleton and of FN expression in cells treated as in D. Nuclei (Nuc) were stained with Hoechst 33342. Scale bars, 50 µm. (F) Cell roundness was measured in 50 individual cells shown as in E, with 1 indicating a perfect circle. Quantitative data represent the mean ± s.d. from three independent experiments, A and D. ***$p < 0.001$; NS, not significant (Student's *t* test).

FN binds to integrins at the cell surface via its Arg-Gly-Asp (RGD) motif (Plow *et al.*, 2000; Singh *et al.*, 2010), and a synthetic RGD peptide inhibits the interaction of cells with a FN matrix (Cardarelli *et al.*, 1994; Avraamides *et al.*, 2008). We therefore next tested the effects of the RGD peptide on DFAT cells cultured on a FN substrate and exposed to inducers of adipocyte differentiation. Treatment with the RGD peptide attenuated the inhibitory effects of FN on reorganization of the actin cytoskeleton into the pattern characteristic of adipocytes, on the expression of adipogenic differentiation genes, and on the accumulation of lipid droplets, whereas a control RGE peptide had no such effects (Figure 3, E–H). These results suggested that release of the interaction between a FN matrix and integrins is required for reorganization of the actin cytoskeleton into the pattern characteristic of adipocytes and for the consequent completion of adipogenesis.

ITGα5 inhibits both reorganization of the actin cytoskeleton into the pattern characteristic of adipocytes and completion of adipogenesis through interaction with the fibronectin matrix

We next analyzed microarray data (GSE156495) to identify integrins that might mediate FN-induced inhibition of actin reorganization

characteristic of adipocytes. Among 16 alpha integrin genes, we found that two genes for RGD-binding integrins (*Itga5* and *Itgav*) were expressed at a high level in undifferentiated DFAT cells but at a low level in mature adipocytes (Supplemental Figure S7A). Integrin expression shifts from FN binding α5 (ITGα5) to laminin binding α6 during adipogenesis has been previously reported (Liu *et al.*, 2005; Pope *et al.*, 2016). We focused our attention on ITGα5, which was also shown to contribute to adipogenesis in 3T3-L1 preadipocytes and human adipose tissue–derived stem cells (Liu *et al.*, 2005; Wang *et al.*, 2010; Morandi *et al.*, 2016). Similarly to FN, expression of ITGα5 at both mRNA and protein levels was detected at a high level in DFAT cells before adipogenic induction and was found to decrease gradually for up to 72 h after exposure of the cells to inducers of adipocyte differentiation, with the cells having become shrunken and stellate and adopted the actin architecture characteristic of adipocytes at 48 h (Figure 4, A–C). These results suggested that ITGα5 might contribute to regulation of such reorganization of the actin cytoskeleton in cooperation with FN. We next investigated the effects of depletion of ITGα5 with specific siRNAs in DFAT cells cultured on a FN substrate and exposed to inducers of adipocyte differentiation. Knockdown of ITGα5 (Supplemental Figure S7B) attenuated the inhibitory effect of the FN matrix on adipocyte
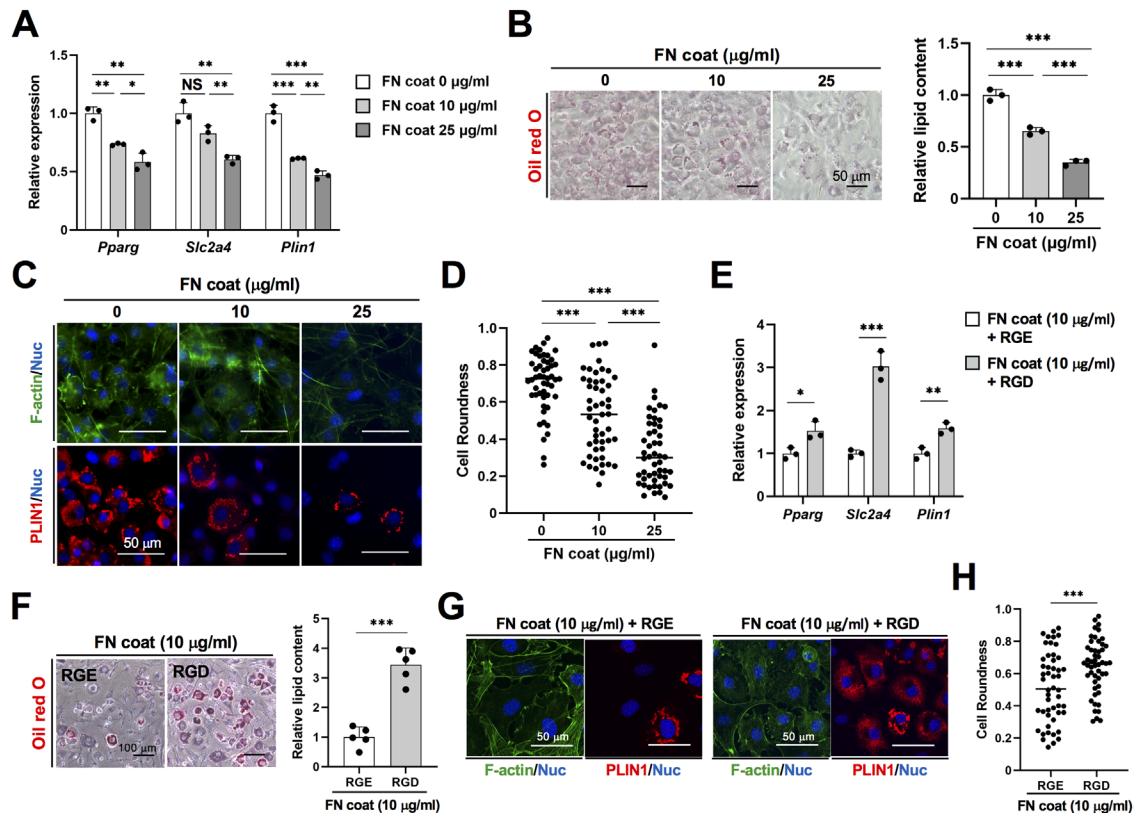
FIGURE 3: FN suppresses reorganization of the actin cytoskeleton into the pattern characteristic of adipocytes as well as completion of adipogenesis in DFAT cells. (A) Relative abundance of *Pparg*, *Slc2a4*, and *Plin1* mRNAs in DFAT cells cultured on plates coated with fibronectin (0, 10, or 25 µg/ml) and exposed to inducers of adipogenesis for 96 h. (B) Cells treated as in A were stained with oil red O (left panels), and relative lipid content was determined by measurement of A_{510} of dye extracted from the stained cells (right panel). Scale bars, 50 µm. (C) Fluorescence microscopy of the actin cytoskeleton (stained with phalloidin) and of PLIN1 expression in cells treated as in A. Nuclei (Nuc) were stained with Hoechst 33342. Scale bars, 50 µm. (D) Cell roundness was measured in 50 individual cells shown as in C, with 1 indicating a perfect circle. (E) Relative abundance of *Pparg*, *Slc2a4*, and *Plin1* mRNAs in DFAT cells cultured on plates coated with fibronectin (10 µg/ml) and exposed to inducers of adipogenesis in the presence of RGD or RGE (control) peptides (100 µg/ml) for 96 h. (F) Oil red O staining and relative lipid content of cells treated as in E. Scale bars 100 µm. (G) Fluorescence microscopy of the actin cytoskeleton and of PLIN1 expression in cells treated as in E. Nuclei were stained with Hoechst 33342. Scale bars, 50 µm. (H) Cell roundness was measured in 50 individual cells shown as in G, with 1 indicating a perfect circle. All quantitative data are means ± s.d. from three – A, B, and E – or five – F – independent experiments. *$p < 0.05$, **$p < 0.01$, ***$p < 0.001$; NS, not significant (Student's *t* test).

differentiation (Figure 4, D–G). In addition, in the absence of inducers of adipogenesis, depletion of ITGα5 alone resulted in a significant increase in the expression of adipogenic differentiation genes, but not in the accumulation of lipid droplets, in DFAT cells (Supplemental Figure S7, C and D). Together, these results thus suggested that the interaction of ITGα5 with FN suppresses actin reorganization characteristic of adipocyte differentiation.

The actin-MKL1 regulatory axis determines expression of ITGα5

MKL1 (also known as MAL or MRTF-A) is a transcriptional coactivator of serum response factor (SRF), and the binding of MKL1 to monomeric G-actin prevents its translocation to the nucleus and thereby inhibits its coactivator function (Miralles *et al.*, 2003; Olson and Nordheim, 2010). We previously showed that depolymerization of the actin cytoskeleton drives adipocyte differentiation by preventing the nuclear translocation of and transcriptional coactivation by MKL1 (Nobusue *et al.*, 2014). It has recently been shown that hypoxia induces the increased expression of FN and ITGα5 in adipocytes as well as the nuclear translocation of MKL1 by increasing actin stress

fiber formation, and resulting in a down-regulation of adipogenic differentiation genes (Anvari and Bellas, 2021), thus suggesting links between MKL1 and FN or ITGα5 in the adipocyte differentiation program. A total of 683 MKL1 target genes was previously identified by chromatin immunoprecipitation and sequencing (ChIP-seq) analysis of SRF-MKL1 binding sites and was found to include genes for RGD-binding integrins (*Itga5* and *Itgav*) (Esnault *et al.*, 2014). Furthermore, MKL1 was shown to regulate expression of the ITGα5 gene by binding to and mediating transactivation of the promoter in NIH3T3 fibroblasts and mesenchymal stem cells (Leitner *et al.*, 2011; Zhang *et al.*, 2015). To test whether inactivation of MKL1 contributes to down-regulation of ITGα5 expression during adipogenesis, we investigated the effect of MKL1 knockdown on ITGα5 expression in DFAT cells. Depletion of MKL1 resulted in a marked decrease in the amounts of both *Itga5* mRNA and ITGα5 protein (Figure 5A). To clarify further the influence of MKL1 on ITGα5 expression, we established DFAT cells that stably express FLAG epitope–tagged versions of either full-length MKL1 (DFAT-TetOn-FLAG-MKL1-WT) or a deletion mutant thereof that lacks the RPEL actin binding domain (Gau and Roy, 2018) (DFAT-TetOn-FLAG-MKL1-N100) under the control of
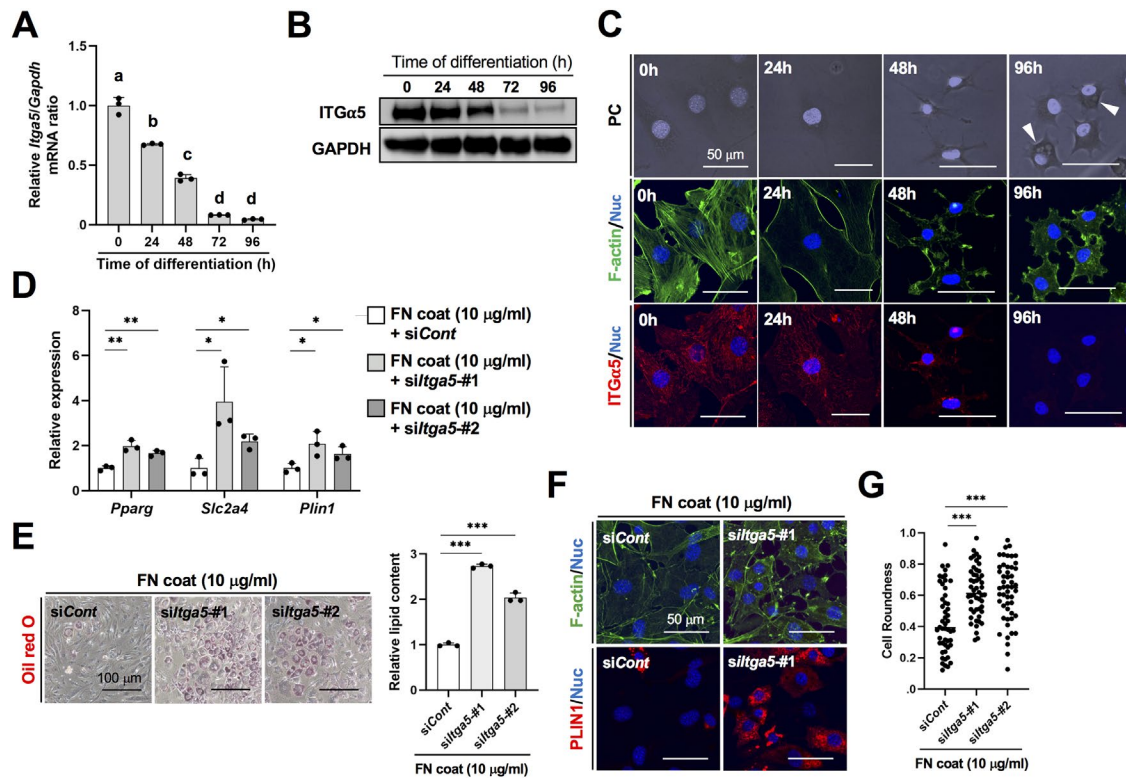
FIGURE 4: ITGα5 regulates actin reorganization characteristic of adipocyte differentiation and the consequent completion of adipogenesis in DFAT cells via interaction with FN. (A) Relative abundance of *Itga5* mRNA during adipocytic differentiation in DFAT cells. $^{a-d}p < 0.05$ (Tukey's honest significant difference test). (B) Immunoblot analysis of ITGα5 during adipocyte differentiation in DFAT cells. (C) Fluorescence microscopy of the actin cytoskeleton (stained with phalloidin) and of ITGα5 expression during adipogenesis in DFAT cells. Nuclei (Nuc) were stained with Hoechst 33342, and phase contrast (PC) images are also shown. Scale bars, 50 μm. Arrowheads indicate cells with lipid droplets. (D) Relative abundance of *Pparg*, *Slc2a4*, and *Plin1* mRNAs in DFAT cells seeded on plates coated with fibronectin (10 μg/ml), transfected with Itga5 (siItga5-#1 or -#2) or control (siCont) siRNAs for 48 h, and then exposed to inducers of adipogenesis for 96 h. (E) Oil red O staining of cells treated as in D, and relative lipid content determined by measurement of A_{510} of dye extracted from the stained cells. Scale bars, 100 μm. (F) Fluorescence microscopy of the actin cytoskeleton and of PLIN1 expression in cells treated as in D. Nuclei were stained with Hoechst 33342. Scale bars, 50 μm. (G) Cell roundness was measured in 50 individual cells shown as in F, with 1 indicating a perfect circle. All quantitative data are means ± s.d. from three independent experiments, A, D, and E. *$p < 0.05$, **$p < 0.01$, ***$p < 0.001$ (Student's *t* test).

the TetOn promoter (Figure 5B). Exposure of both these cell lines to the TetOn inducer doxycycline resulted in a marked increase in the expression of ITGα5 at both mRNA and protein levels (Figure 5C). Treatment with the actin-depolymerizing agent latrunculin A (LatA), which increases the abundance of monomeric G-actin (Coue *et al.*, 1987; Miralles *et al.*, 2003), prevented these effects of doxycycline in DFAT-TetOn-FLAG-MKL1-WT cells but not in DFAT-TetOn-FLAG-MKL1-N100 cells (Figure 5C). In addition, expression of *Fn1* was found not to be directly controlled by MKL1 in DFAT cells (Supplemental Figure S8). Together, these findings indicated that MKL1 mediates up-regulation of ITGα5 expression in DFAT cells, and that this action is impaired by its interaction with G-actin (Figure 5D).

DISCUSSION
FN binds to integrins, including α5β1, that recognize the RGD motif, and these integrins interact with the actin cytoskeleton via the integrin activator talin and thereby regulate actin dynamics and many cellular processes (Jiang *et al.*, 2003; Moser *et al.*, 2009). FN has been shown to promote activation of members of the Rho family of small GTPases as well as formation of actin stress fibers in cultured cells (Bourdoulous *et al.*, 1998; Bloom *et al.*, 1999). On the other hand, lysophosphatidic

acid (LPA)–mediated Rho activation results in the formation of actin stress fibers as well as promoting FN matrix assembly, whereas actin depolymerization attenuates LPA-induced matrix assembly (Zhang *et al.*, 1994, 1997), suggesting that the formation of actin stress fibers and FN matrix assembly are functionally linked through inside-out or outside-in signaling. We have now shown that exposure of DFAT cells to an adipogenic cocktail resulted in the rapid depolymerization of actin stress fibers followed by the disruption of fibrillar FN structures and the eventual disappearance of FN. We previously showed that such actin depolymerization is sufficient to elicit adipocyte differentiation of several progenitor cells in the absence of an adipogenic cocktail (Nobusue *et al.*, 2014; Takahashi *et al.*, 2019; Kunitomi *et al.*, 2020). We also found that treatment with phalloidin (a cytoskeletal fixative) blocked the depolymerization of actin stress fibers as well as the disruption of fibrillar FN structures in DFAT cells exposed to inducers of adipocytic differentiation (Supplemental Figure S9A). Furthermore, expression of hemagglutinin epitope (HA)–tagged dominant active RhoA mutant (RhoAV14) inhibited remodeling both of actin stress fibers and of fibrillar FN structures in DFAT cells exposed to inducers of adipocytic differentiation, unlike that of dominant negative RhoA mutant (RhoAN19), and these inhibitory effects were prevented
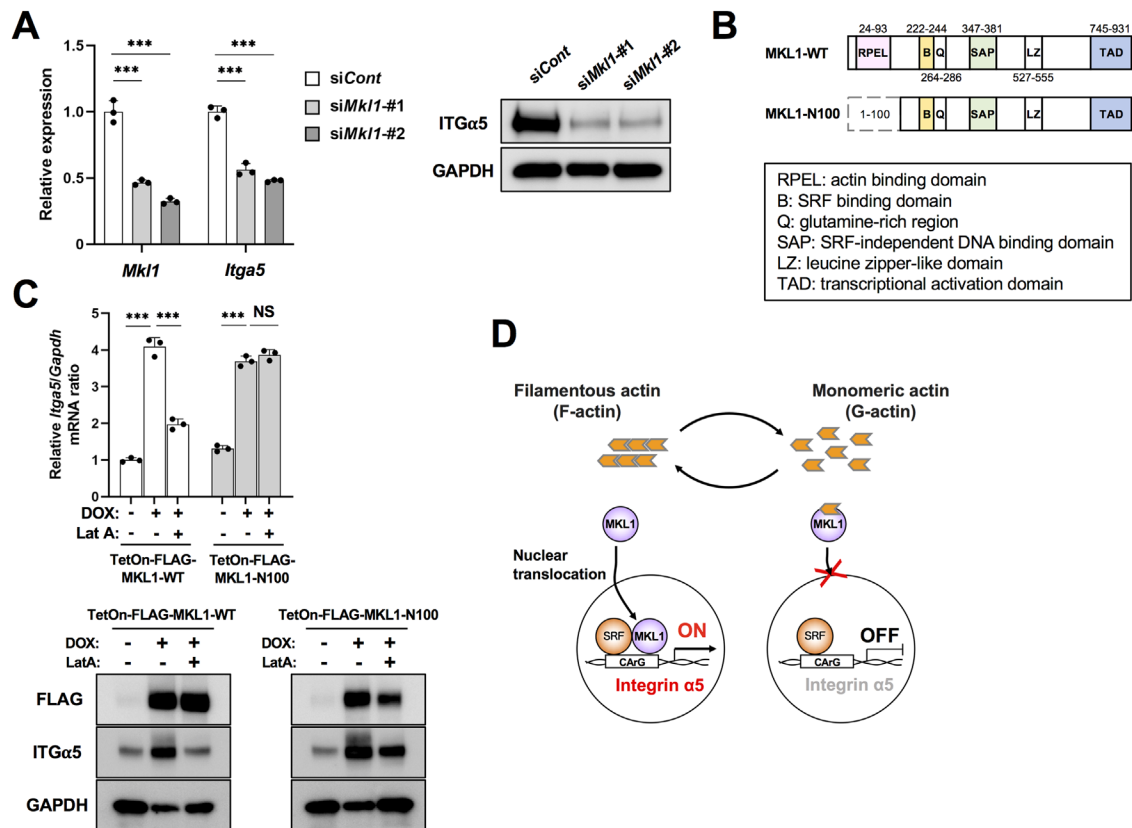
FIGURE 5: The actin–MKL1 pathway regulates expression of ITGα5 in DFAT cells. (A) Relative abundance of *Mkl1* and *Itga5* mRNAs (left) and immunoblot analysis of ITGα5 (right) in DFAT cells transfected with *Mkl1* (si*Mkl1*-#1 or -2#) or control (si*Cont*) siRNAs for 48 h. (B) Domain organization of wild-type (WT) and mutant (N100) forms of MKL1. (C) Relative abundance of *Itga5* mRNA in DFAT-TetOn-FLAG-MKL1-WT or DFAT-TetOn-FLAG-MKL1-N100 cells exposed for 24 h to LatA (0.4 µM) or doxycycline (DOX, 1 µg/ml) as indicated (Upper). The cells were also subjected to immunoblot analysis of FLAG and ITGα5 (Lower). All quantitative data are means ± s.d. from three independent experiments. ***$p < 0.001$; NS, not significant (Student's *t* test). (D) Model for regulation of ITGα5 expression by the actin-MKL1 pathway. The CArG box is the consensus binding sequence for the SRF-MKL1 complex.

by treatment with Rho-associated coiled-coil containing protein kinase (ROCK) inhibitor Y-27632 (Supplemental Figure S9B). Our findings thus suggest that adipogenic stimuli elicit disruption of fibrillar FN structures indirectly, with this effect being mediated by a cue from inside of the cell to outside that is dependent on the depolymerization of actin stress fibers.

ECM degradation is mediated by a family of zinc-dependent proteases known as matrix metalloproteinases (MMPs) (Kessenbrock *et al.*, 2010). MMPs are synthesized as inactive proenzymes and are activated as a result of proteolytic removal of the pro domain by plasmin. The expression and secretion of MMP-2 and MMP-9 increase during adipocyte differentiation in human preadipocytes and 3T3-F442A mouse preadipocytes, and inhibition of these MMP activities attenuates adipogenesis (Bouloumie *et al.*, 2001; Croissandeau *et al.*, 2002). In particular, MMP-2 contributes to adipocyte differentiation through degradation of FN (Croissandeau *et al.*, 2002). We found that the abundance of *Mmp2* mRNA was transiently increased between 24 and 48 h after the induction of adipocyte differentiation in DFAT cells (Supplemental Figure S10A). Gelatin zymography also revealed that the activities of both proMMP-2 and MMP-2 were markedly increased at 48 h (Supplemental Figure S10B), at which time loss of the fibrillar FN structures at the cell surface was complete (Figure 1C). Together, these results implicate MMP-2 in the degradation of FN that occurs after disruption of the fibrillar structures during adipogenesis.

The switch from α5 to α6 integrins is recognized as one of the important events of the adipocyte differentiation program (Liu *et al.*, 2005; Pope *et al.*, 2016). Overexpression of ITGα5 has been shown to inhibit adipocyte differentiation, with knockdown of ITGα5 resulting in enhancement of adipogenesis (Liu *et al.*, 2005; Wang *et al.*, 2010; Morandi *et al.*, 2016), indicating that ITGα5 acts as a negative factor in adipocyte differentiation. In the present study, we clarified a novel role of ITGα5 in controlling reorganization of the actin cytoskeleton from depolymerized actin to the pattern characteristic of adipocytes. Furthermore, we found that the expression of ITGα5 is directly controlled by MKL1 in DFAT cells, and that knockdown of ITGα5 alone induced the up-regulation of adipogenic differentiation genes in the absence of an adipogenic cocktail, similarly to MKL1 depletion (Nobusue *et al.*, 2014). Our findings thus suggest that ITGα5 itself acts as a functional regulator for the MKL1-mediated adipocyte differentiation program.

PPARγ is a member of the nuclear receptor superfamily and drives the expression of downstream target genes that are necessary for the generation and maintenance of adipocyte characteristics such as lipid accumulation and insulin sensitivity. It is thus thought to function as a master regulator in acquisition of the adipocytic phenotype (Rosen *et al.*, 2000; Rosen and MacDougald, 2006). We have now shown that PPARγ negatively regulates FN expression during adipocyte differentiation. Thiazolidinedione-mediated activation or overexpression of PPARγ was previously found to inhibit the expression
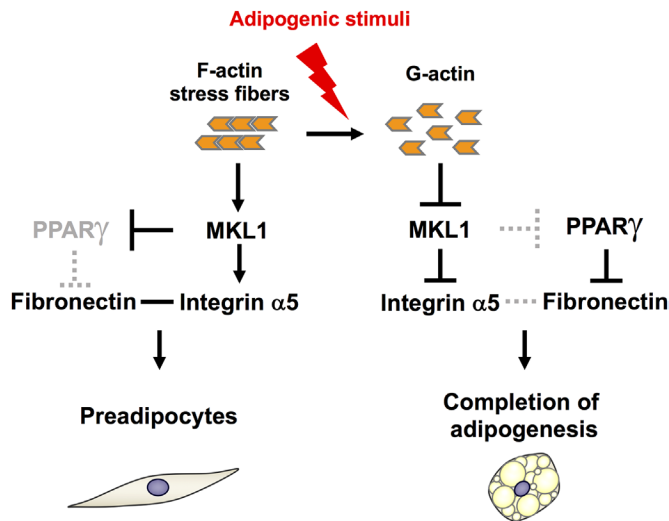
FIGURE 6: Proposed mechanism underlying regulation of cell–matrix interaction during the differentiation of progenitor cells into adipocytes. Preadipocytes manifest a high level of FN expression as well as well-developed actin stress fibers, with the result that MKL1 is activated and maintains a high level of ITGα5 expression. Adipogenic stimulation induces depolymerization of actin stress fibers and attenuates the transcriptional regulatory activity of MKL1 as a consequence of its binding to monomeric G-actin. The inhibition of MKL1 activity results in down-regulation of ITGα5, and the initiation of PPARγ expression leads to down-regulation of FN. The loss of FN and ITGα5 allows reorganization of the actin cytoskeleton into the pattern characteristic of adipocytes and completion of adipocyte differentiation.

of FN in mouse glomerular mesangial cells or human lung carcinoma cells (Guo *et al.*, 2004; Han *et al.*, 2005). Together, these observations suggest that PPARγ contributes to the control not only of adipocyte-specific gene expression but also of reorganization of the ECM associated with the adipocyte differentiation program. In addition, we previously showed that MKL1 and PPARγ act in a mutually antagonistic manner in the adipocyte differentiation program (Nobusue *et al.*, 2014), implicating this mutual antagonism to be a determinant of the reorganization of ECM structure that is required for the differentiation of progenitor cells into adipocytes.

In conclusion, our results provide new insight into the regulation of cell–matrix interaction during the adipocyte differentiation program (Figure 6). Preadipocytes manifest a high level of FN expression as well as well-developed actin stress fibers, with the result that MKL1 is activated and maintains expression of ITGα5 also at a high level. Exposure of preadipocytes to an adipogenic cocktail (adipogenic stimuli) induces depolymerization of actin stress fibers as well as inhibition of the transcriptional regulatory activity of MKL1 as a consequence of its binding to monomeric G-actin. The loss of MKL1 activity results in down-regulation of ITGα5, and the initiation of PPARγ expression leads to down-regulation of FN. The loss of FN and ITGα5 allows reorganization of the actin cytoskeleton into the pattern characteristic of adipocytes and completion of adipocyte differentiation. The cell differentiation is completed by the inside-to-outside-to-inside signal; the actin reorganization induces changes in the ECM composition, which in turn drives intracellular transcription and shape changes. Last, given that cell density/confluency is known to have significant effects on the cytoskeletal organization and cellular differentiation (McBeath *et al.*, 2004; Panciera *et al.*, 2017), it needs to be further investigated.

MATERIALS AND METHODS
Request a protocol through *Bio-protocol*.

Cell culture
The mouse DFAT cell line was established from mature adipocytes by ceiling culture as described previously (Nobusue *et al.*, 2008). The mouse embryonic 3T3-L1 preadipocyte cell line was obtained from the Japanese Collection of Research Bioresources (Tokyo, Japan). The human HPAd preadipocyte cell line derived from subcutaneous tissue was purchased from Cell Applications (San Diego, CA). The 3T3-L1 and HPAd cell lines were frozen down at two passages and used in the experiments within five passages after thawing. These cells were authenticated by examination of in vitro growth characteristics and morphology properties provided evidence of correct cell identity. All cells were regularly tested as mycoplasma-free by PCR. DFAT and 3T3-L1 cells were cultured under 5% CO_2 at 37°C in DMEM (Nacalai Tesque, Kyoto, Japan) supplemented with 10% fetal bovine serum (FBS) and penicillin–streptomycin (Nacalai Tesque). HPAd cells were cultured with HPAd growth medium (Cell Applications). For adipocyte differentiation, all cells were grown to 80% confluency and then cultured in DMEM supplemented with 10% FBS, 0.5 mM 3-isobutyl-1-methylxanthine (Nacalai Tesque), 0.1 µM dexamethasone (Wako, Osaka, Japan), and insulin-transferrin-selenium-X (final insulin concentration of 5 µg/ml) (Thermo Fisher Scientific, Waltham, MA). After 7 d, in HPAd cells, the differentiation medium was replaced with DMEM supplemented with 1% bovine serum albumin (BSA; Sigma-Aldrich, St. Louis, MO) and ITS for 7 d (total 14 d).

Soft ECM
CytoSoft imaging 24-well plates (2 kPa elastic modulus; Advanced-BioMatrix, San Diego, CA) were coated overnight at 37°C with poly-L-ornithine (Sigma-Aldrich) at 100 µg/ml in phosphate-buffered saline (PBS) and washed three times with PBS.

Fibronectin coating
Sterile glass coverslips (Matsunami, Osaka, Japan) were placed in the wells of a six-well plate (Corning, Corning, NY), coated overnight at 37°C with poly-L-ornithine (Sigma-Aldrich) at 100 µg/ml in PBS, washed three times with PBS, coated overnight at 37°C with FN (Wako) at 0 to 25 µg/ml in PBS, and finally washed another three times with PBS.

Cell proliferation assay
Cells were counted with the Countess 3 automated cell counter (Thermo Fisher Scientific). Live cells were identified by staining with trypan blue (Sigma-Aldrich). All assays were performed in quadruplicate.

Reverse transcription and real-time polymerase chain reaction analysis
Total RNA was isolated from cells with the TRIzol reagent (Thermo Fisher Scientific), and portions (500 ng) of the RNA were subjected to RT with SuperScript VILO Master Mix (Thermo Fisher Scientific). Real-time PCR analysis was performed in triplicate with TaqMan Fast Universal PCR Master Mix (Thermo Fisher Scientific) and a StepOnePlus thermocycler (Thermo Fisher Scientific). The probes for mouse *Pparg* (GenBank accession no. NM_011146.3; Mm00440940_m1), mouse *Plin1* (NM_17564.2; Mm00558672_m1), mouse *Mkl1* (NM_153049.2; Mm00461840_m1), mouse *Slc2a4* (NM_009204.2; Mm01245502_m1), mouse *Fn1* (NM_001276408.1; Mm01256744_m1), mouse *Itga5* (NM_010577.3; Mm00439797_m1), mouse *Mmp2*

(NM_008610.2; Mm00439506_m1), human *PPARG* (GenBank accession no. NM_015869.4; Hs01115513_m1), human *PLIN1* (GenBank accession no. NM_001145311.1; Hs0016017_m1), and human *SLC2A4* (GenBank accession no. NM_001042.2.; Hs00168966_m1) were obtained as TaqMan predeveloped assay reagents (Thermo Fisher Scientific). A mouse *Gapdh* (NM_008084.2) TaqMan probe (4352339E, Thermo Fisher Scientific) or eukaryotic 18S rRNA (X03205.1) TaqMan probe (4319413E, Thermo Fisher Scientific) was included as an endogenous control.

Immunoblot analysis

Immunoblot analysis was performed according to standard procedures (Nobusue *et al.*, 2014) with rabbit polyclonal antibodies to FN (1:1000 dilution; F3648, Sigma-Aldrich), rabbit monoclonal antibodies to ITGα5 (1:500 dilution; ab150361; Abcam, Cambridge, MA), and mouse monoclonal antibodies to FLAG (1:500 dilution; F1804, Sigma-Aldrich) and to GAPDH (1:1000 dilution; 60004-1-Ig; Proteintech, Chicago, IL). Uncropped scans of the most important western blots were shown in Supplementary data.

Zymography

Cells were washed extensively with PBS and then subjected to extraction of a crude protein fraction with the M-PER mammalian protein extraction reagent (Thermo Fisher Scientific) in the presence of a protease inhibitor cocktail (Nacalai Tesque). The crude protein fraction (10 µg) was mixed with Novex tris-glycine sodium dodecyl sulfate (SDS) sample buffer (Thermo Fisher Scientific) and subjected to electrophoresis on a 10% Zymogram (gelatin gel, Thermo Fisher Scientific). The gel was washed with Zymogram renaturing buffer (Thermo Fisher Scientific) for 1 h and then incubated at 37°C for 48 h with Zymogram developing buffer (Thermo Fisher Scientific), after which the activity of MMP-2 was visualized by staining with Coomassie Brilliant Blue R-250 (Wako).

Fluorescence microscopy

Cells were washed three times with PBS, fixed for 15 min at room temperature with 4% paraformaldehyde, washed with PBS, and incubated for 1 h at room temperature with 1% normal goat serum (Wako) and 1% BSA (Sigma-Aldrich) in PBS to block nonspecific binding of antibodies before staining with primary antibodies according to standard procedures. Primary antibodies included rabbit monoclonal antibodies to ITGα5 (1:200 dilution; ab150361, Abcam) as well as rabbit polyclonal antibodies to perilipin A/B (1:500 dilution; P1873, Sigma-Aldrich) and to FN (1:800 dilution; F3648, Sigma-Aldrich). Secondary antibodies conjugated with Alexa Fluor 488 or Alexa Fluor 594 were obtained from Molecular Probes (Eugene, OR). F-actin was stained with Alexa Fluor 488– or Alexa Fluor 594–labeled phalloidin (200 U/ml, Molecular Probes) in PBS. Cells were counterstained with Hoechst 33342 (Sigma-Aldrich) at 5 µg/ml and were observed with an FV10i confocal laser-scanning microscope (Olympus, Tokyo, Japan). Using the images of the actin cytoskeleton, the cell boundary was manually traced and the roundness ($4 \times$ area/[$\pi \times$ major axis length^2]) of the individual cells was quantified with ImageJ/FIJI software (National Institutes of Health, Bethesda, MD).

Lipid staining

Lipid accumulation in adipocytes was detected by staining with oil red O (Wako). Cells were washed three times with PBS, fixed for 1 h at room temperature with 10% formalin in phosphate buffer, washed again with PBS, and stained for 15 min at room temperature with a filtered solution of oil red O (0.5 g in 100 ml of isopropyl alcohol).

The cells were then washed twice with distilled water for 15 min. For quantitation of lipid accumulation, dimethyl sulfoxide (DMSO; 500 µl per 35-mm dish) was added to the washed and dried cells for 1 min, after which the absorbance of the extracted dye at 510 nm (A_{510}) was measured with a spectrophotometer (ND-1000; Nanodrop Technologies, Wilmington, DE) and was normalized by dish area.

Pharmacological reagents

Cells were exposed to the following reagents: phalloidin oleate (Calbiochem, San Diego, CA) at 5 µM in DMSO, Y-27632 (Calbiochem) at 30 µM in H$_2$O, GRGDSP (RGD peptide; Takara, Kyoto, Japan) or GRGESP (RGE peptide, Takara) at 100 µg/ml in H$_2$O, or doxycycline (Sigma-Aldrich) at 1 µg/ml in H$_2$O, 0.4 µM LatA (Calbiochem) in DMSO.

Plasmid transfection

The pEF-BOS-HA-RhoAV14 and pEF-BOS-HA-RhoAN19 (Amano *et al.*, 1996) plasmids were transfected into DFAT cells for 24 h using the FugeneHD reagent (Promega, Madison, WI).

RNA interference

Expression of shRNAs was achieved with the retroviral expression vector pRePs (kindly provided by T. Hara, Tokyo Metropolitan Institute of Medical Science, Tokyo, Japan), which also contains a puromycin resistance gene. The sequences of the sense oligonucleotides were 5′-GTTTGAGTTTGCTGTGAAG-3′ for the PPARγ shRNA (Shimizu *et al.*, 2010) and 5′-CGTACGCGGAATACTTCGA-3′ for the luciferase shRNA (nonspecific control). The pRePs vectors were introduced into Plat-E packaging cells (Fujino *et al.*, 2006) by transfection for 24 h with the use of the FugeneHD reagent (Promega). Culture supernatants collected after a second incubation of the cells for 24 h were passed through a 0.45-µm cellulose acetate filter (Iwaki, Chiba, Japan) to obtain the generated retroviruses. Retroviral infection of DFAT cells was performed with cells in a six-well plate for 48 h and was followed by selection in the presence of puromycin (10 µg/ml). The sequences of siRNAs were 5′-AUCUGGGACGGCUUGUCAAUUUCUG-3′ for *Fn1*-#1, 5′- UAAUAGUGAUGGUGGUCUCUGUAGC-3′ for *Fn1*-#2, 5′-CCGUUUCAAAUAGUCCUCGGU-3′ for *Mkl1*-#1, 5′-GAGAAAGAACCUGAGUGGGUG-3′ for *Mkl1*-#2, 5′-GAAUGAAUCAGAAUUCAGAGA-3′ for *Itga5*-#1, and 5′-CUACACUACCAAAGCAAAAGC-3′ for *Itga5*-#2. The control siRNA sequence was 5′-GCGCGCUUUGUAGGAUUCG-3′. Cells were transfected with siRNA duplexes for 48 h with the use of Lipofectamine RNAiMAX (Thermo Fisher Scientific).

Retroviral gene transfers

The immortalization of HPAd was achieved with the retroviral expression vector pBABE-puro-hTERT (provided by B. Weinberg; Addgene, #1771; Counter *et al.*, 1998). GP2-293 packaging cells (Clontech) were transfected with the pBABE-puro-hTERT and the VSV-G envelope plasmid pCMV-VSV-G (provided by B. Weinberg; Addgene, #8454; Stewart *et al.*, 2003) with FugeneHD reagent (Promega), after which recombinant retroviruses were collected and HPAd were infected with the retroviruses and subjected to selection as described above for RNA interference. The cDNAs for wild type and a constitutively active mutant (N100) of human MKL1 were obtained by digestion of Addgene plasmids #11978 and #27176 (Cen *et al.*, 2003), respectively, with *Eco*RI and *Bam*HI, and the released fragments were cloned into the *Eco*RI and *Bam*HI sites of the custom pRetroX-3 × FLAG-Tight-Pur vector (Masuda *et al.*, 2015) to yield pRetroX-3 × FLAG-tagged MKL1-Tight-Pur and pRetroX-3 × FLAG-tagged MKL1-N100-Tight-Pur. The retroviral vectors were

introduced into Plat-E packaging cells (Morita *et al.*, 2000), recombinant retroviruses were collected, and cells were infected with the retroviruses and subjected to selection as described above for RNA interference. For generation of DFAT-TetOn-FLAG-MKL1-WT and DFAT-TetOn-FLAG-MKL1-N100 cells, DFAT cells were infected with the pRetroX-Tet-on Advanced-hygro response virus for 48 h (Masuda *et al.*, 2015) and then subjected to selection in the presence of hygromycin (200 μg/ml). Cells resistant to hygromycin were then infected with the pRetroX-3 × FLAG-tagged MKL1-Tight-Pur or pRetroX-3 × FLAG-tagged MKL1-N100-Tight-Pur viruses for 48 h and subjected to selection with puromycin (10 μg/ml).

Analysis of microarray data

The microarray data are accessible through GEO series accession number GSE156495 (Hagiwara *et al.*, 2020) for DFAT and Adipocyte. 3T3-L1 and C310T1/2 microarray data sets (GSM258609, GSM258610, GSM258631 and GSM25832) were also obtained from GEO. Expression and raw expression data (CEL files) were summarized and normalized with the use of the Robust Multi-array Average algorithm and the Bioconductor package affy (http://www.bioconductor.org/packages/2.0/bioc/html/affy.html). The Spotfire DecisionSite for Functional Genomics software package (TIBCO Software, Palo Alto, CA) was used for visualization of the microarray data.

Statistical analysis

Data are presented as means ± s.d. and were analyzed with Tukey's honest significant difference test or Student's t test for comparisons between two or among three or more groups, respectively. A p value of <0.05 was considered statistically significant.

REFERENCES

Amano M, Ito M, Kimura K, Fukata Y, Chihara K, Nakano T, Matsuura Y, Kaibuchi K (1996). Phosphorylation and activation of myosin by Rho-associated kinase (Rho-kinase)*. J Biol Chem 271, 20246–20249.

Anvari G, Bellas E (2021). Hypoxia induces stress fiber formation in adipocytes in the early stage of obesity. Sci Rep 11, 21473.

Avraamides CJ, Garmy-Susini B, Varner JA (2008). Integrins in angiogenesis and lymphangiogenesis. Nat Rev Cancer 8, 604–617.

Blache U, Stevens MM, Gentleman E (2020). Harnessing the secreted extracellular matrix to engineer tissues. Nat Biomed Eng 4, 357–363.

Bloom L, Ingham KC, Hynes RO (1999). Fibronectin regulates assembly of actin filaments and focal contacts in cultured cells via the heparin-binding site in repeat III13. Mol Biol Cell 10, 1521–1536.

Bonnans C, Chou J, Werb Z (2014). Remodelling the extracellular matrix in development and disease. Nat Rev Mol Cell Biol 15, 786–801.

Bouloumie A, Sengenes C, Portolan G, Galitzky J, Lafontan M (2001). Adipocyte produces matrix metalloproteinases 2 and 9: involvement in adipose differentiation. Diabetes 50, 2080–2086.

Bourdoulous S, Orend G, MacKenna DA, Pasqualini R, Ruoslahti E (1998). Fibronectin matrix regulates activation of RHO and CDC42 GTPases and cell cycle progression. J Cell Biol 143, 267–276.

Cardarelli PM, Cobb RR, Nowlin DM, Scholz W, Gorcsan F, Moscinski M, Yasuhara M, Chiang SL, Lobl TJ (1994). Cyclic RGD peptide inhibits alpha 4 beta 1 interaction with connecting segment 1 and vascular cell adhesion molecule. J Biol Chem 269, 18668–18673.

Cen B, Selvaraj A, Burgess RC, Hitzler JK, Ma Z, Morris SW, Prywes R (2003). Megakaryoblastic leukemia 1, a potent transcriptional coactivator for serum response factor (SRF), is required for serum induction of SRF target genes. Mol Cell Biol 23, 6597–6608.

Coue M, Brenner SL, Spector I, Korn ED (1987). Inhibition of actin polymerization by latrunculin A. FEBS Lett 213, 316–318.

Counter CM, Meyerson M, Eaton EN, Ellisen LW, Caddle SD, Haber DA, Weinberg RA (1998). Telomerase activity is restored in human cells by ectopic expression of hTERT (hEST2), the catalytic subunit of telomerase. Oncogene 16, 1217–1222.

Cristancho AG, Lazar MA (2011). Forming functional fat: a growing understanding of adipocyte differentiation. Nat Rev Mol Cell Biol 12, 722–734.

Croissandeau G, Chretien M, Mbikay M (2002). Involvement of matrix metalloproteinases in the adipose conversion of 3T3-L1 preadipocytes. Biochem J 364, 739–746.

Desgrosellier JS, Cheresh DA (2010). Integrins in cancer: biological implications and therapeutic opportunities. Nat Rev Cancer 10, 9–22.

Discher DE, Mooney DJ, Zandstra PW (2009). Growth factors, matrices, and forces combine and control stem cells. Science 324, 1673–1677.

Engler AJ, Sen S, Sweeney HL, Discher DE (2006). Matrix elasticity directs stem cell lineage specification. Cell 126, 677–689.

Esnault C, Stewart A, Gualdrini F, East P, Horswell S, Matthews N, Treisman R (2014). Rho-actin signaling to the MRTF coactivators dominates the immediate transcriptional response to serum in fibroblasts. Genes Dev 28, 943–958.

Fujino RS, Tanaka K, Morimatsu M, Tamura K, Kogo H, Hara T (2006). Spermatogonial cell-mediated activation of an IkappaBzeta-independent nuclear factor-kappaB pathway in Sertoli cells induces transcription of the lipocalin-2 gene. Mol Endocrinol 20, 904–915.

Gattazzo F, Urciuolo A, Bonaldo P (2014). Extracellular matrix: a dynamic microenvironment for stem cell niche. Biochim Biophys Acta 1840, 2506–2519.

Gau D, Roy P (2018). SRF'ing and SAP'ing – the role of MRTF proteins in cell migration. J Cell Sci 131, jcs218222.

Guilak F, Cohen DM, Estes BT, Gimble JM, Liedtke W, Chen CS (2009). Control of stem cell fate by physical interactions with the extracellular matrix. Cell Stem Cell 5, 17–26.

Guo B, Koya D, Isono M, Sugimoto T, Kashiwagi A, Haneda M (2004). Peroxisome proliferator-activated receptor-gamma ligands inhibit TGF-beta 1-induced fibronectin expression in glomerular mesangial cells. Diabetes 53, 200–208.

Hagiwara R, Oki Y, Matsumaru T, Ibayashi S, Kano K (2020). Generation of metabolically functional hepatocyte-like cells from dedifferentiated fat cells by Foxa2, Hnf4a and Sall1 transduction. Genes Cells 25, 811–824.

Han S, Ritzenthaler JD, Rivera HN, Roman J (2005). Peroxisome proliferator-activated receptor-gamma ligands suppress fibronectin gene expression in human lung carcinoma cells: involvement of both CRE and Sp1. Am J Physiol Lung Cell Mol Physiol 289, L419–L428.

Hoshiba T, Chen G, Endo C, Maruyama H, Wakui M, Nemoto E, Kawazoe N, Tanaka M (2016). Decellularized extracellular matrix as an in vitro model to study the comprehensive roles of the ECM in stem cell differentiation. Stem Cells Int 2016, 6397820.

Ivanovska IL, Shin JW, Swift J, Discher DE (2015). Stem cell mechanobiology: diverse lessons from bone marrow. Trends Cell Biol 25, 523–532.

Jiang G, Giannone G, Critchley DR, Fukumoto E, Sheetz MP (2003). Two-piconewton slip bond between fibronectin and the cytoskeleton depends on talin. Nature 424, 334–337.

Kessenbrock K, Plaks V, Werb Z (2010). Matrix metalloproteinases: regulators of the tumor microenvironment. Cell 141, 52–67.

Kunitomi H, Oki Y, Onishi N, Kano K, Banno K, Aoki D, Saya H, Nobusue H (2020). The insulin-PI3K-Rac1 axis contributes to terminal adipocyte differentiation through regulation of actin cytoskeleton dynamics. Genes Cells 25, 165–174.

Kwon J, Lee TS, Lee HW, Kang MC, Yoon HJ, Kim JH, Park JH (2013). Integrin alpha 6: a novel therapeutic target in esophageal squamous cell carcinoma. Int J Oncol 43, 1523–1530.

Leitner L, Shaposhnikov D, Mengel A, Descot A, Julien S, Hoffmann R, Posern G (2011). MAL/MRTF-A controls migration of non-invasive cells by upregulation of cytoskeleton-associated proteins. J Cell Sci 124, 4318–4331.

Lilla J, Stickens D, Werb Z (2002). Metalloproteases and adipogenesis: a weighty subject. Am J Pathol 160, 1551–1554.

Liu J, DeYoung SM, Zhang M, Zhang M, Cheng A, Saltiel AR (2005). Changes in integrin expression during adipocyte differentiation. Cell Metab 2, 165–177.

Ma W, Tavakoli T, Derby E, Serebryakova Y, Rao MS, Mattson MP (2008). Cell–extracellular matrix interactions regulate neural differentiation of human embryonic stem cells. BMC Dev Biol 8, 90.

Masuda K, Chiyoda T, Sugiyama N, Segura-Cabrera A, Kabe Y, Ueki A, Banno K, Suematsu M, Aoki D, Ishihama Y, et al. (2015). LATS1 and LATS2 phosphorylate CDC26 to modulate assembly of the tetratricopeptide repeat subcomplex of APC/C. PLoS One 10, e0118662.

McBeath R, Pirone DM, Nelson CM, Bhadriraju K, Chen CS (2004). Cell shape, cytoskeletal tension, and RhoA regulate stem cell lineage commitment. Dev Cell 6, 483–495.

Miralles F, Posern G, Zaromytidou AI, Treisman R (2003). Actin dynamics control SRF activity by regulation of its coactivator MAL. Cell 113, 329–342.

Morandi EM, Verstappen R, Zwierzina ME, Geley S, Pierer G, Ploner C (2016). ITGAV and ITGA5 diversely regulate proliferation and adipogenic differentiation of human adipose derived stem cells. Sci Rep 6, 28889.

Moreira AM, Pereira J, Melo S, Fernandes MS, Carneiro P, Seruca R, Figueiredo J (2020). The extracellular matrix: an accomplice in gastric cancer development and progression. Cells 9, 394.

Morita S, Kojima T, Kitamura T (2000). Plat-E: an efficient and stable system for transient packaging of retroviruses. Gene Ther 7, 1063–1066.

Moser M, Legate KR, Zent R, Fassler R (2009). The tail of integrins, talin, and kindlins. Science 324, 895–899.

Mouw JK, Ou G, Weaver VM (2014). Extracellular matrix assembly: a multiscale deconstruction. Nat Rev Mol Cell Biol 15, 771–785.

Nobusue H, Endo T, Kano K (2008). Establishment of a preadipocyte cell line derived from mature adipocytes of GFP transgenic mice and formation of adipose tissue. Cell Tissue Res 332, 435–446.

Nobusue H, Onishi N, Shimizu T, Sugihara E, Oki Y, Sumikawa Y, Chiyoda T, Akashi K, Saya H, Kano K (2014). Regulation of MKL1 via actin cytoskeleton dynamics drives adipocyte differentiation. Nat Commun 5, 3368.

Ojima K, Oe M, Nakajima I, Muroya S, Nishimura T (2016). Dynamics of protein secretion during adipocyte differentiation. FEBS Open Bio 6, 816–826.

Olson EN, Nordheim A (2010). Linking actin dynamics and gene transcription to drive cellular motile functions. Nat Rev Mol Cell Biol 11, 353–365.

Panciera T, Azzolin L, Cordenonsi M, Piccolo S (2017). Mechanobiology of YAP and TAZ in physiology and disease. Nat Rev Mol Cell Biol 18, 758–770.

Plow EF, Haas TA, Zhang L, Loftus J, Smith JW (2000). Ligand binding to integrins. J Biol Chem 275, 21785–21788.

Pope BD, Warren CR, Parker KK, Cowan CA (2016). Microenvironmental control of adipocyte fate and function. Trends Cell Biol 26, 745–755.

Rosen ED, MacDougald OA (2006). Adipocyte differentiation from the inside out. Nat Rev Mol Cell Biol 7, 885–896.

Rosen ED, Walkey CJ, Puigserver P, Spiegelman BM (2000). Transcriptional regulation of adipogenesis. Genes Dev 14, 1293–1307.

Shimizu T, Ishikawa T, Sugihara E, Kuninaka S, Miyamoto T, Mabuchi Y, Matsuzaki Y, Tsunoda T, Miya F, Morioka H, et al. (2010). c-MYC overexpression with loss of Ink4a/Arf transforms bone marrow stromal cells into osteosarcoma accompanied by loss of adipogenesis. Oncogene 29, 5687–5699.

Singh P, Carraher C, Schwarzbauer JE (2010). Assembly of fibronectin extracellular matrix. Annu Rev Cell Dev Biol 26, 397–419.

Smas CM, Sul HS (1995). Control of adipocyte differentiation. Biochem J 309 (Pt 3), 697–710.

Spiegelman BM, Ginty CA (1983). Fibronectin modulation of cell shape and lipogenic gene expression in 3T3-adipocytes. Cell 35, 657–666.

Stewart SA, Dykxhoorn DM, Palliser D, Mizuno H, Yu EY, An DS, Sabatini DM, Chen IS, Hahn WC, Sharp PA, et al. (2003). Lentivirus-delivered stable gene silencing by RNAi in primary cells. RNA 9, 493–501.

Takahashi N, Nobusue H, Shimizu T, Sugihara E, Yamaguchi-Iwai S, Onishi N, Kunitomi H, Kuroda T, Saya H (2019). ROCK inhibition induces terminal adipocyte differentiation and suppresses tumorigenesis in chemoresistant osteosarcoma cells. Cancer Res 79, 3088–3099.

Wang Y, Zhao L, Smas C, Sul HS (2010). Pref-1 interacts with fibronectin to inhibit adipocyte differentiation. Mol Cell Biol 30, 3480–3492.

Yagi K, Kondo D, Okazaki Y, Kano K (2004). A novel preadipocyte cell line established from mouse adult mature adipocytes. Biochem Biophys Res Commun 321, 967–974.

Zhang Q, Checovich WJ, Peters DM, Albrecht RM, Mosher DF (1994). Modulation of cell surface fibronectin assembly sites by lysophosphatidic acid. J Cell Biol 127, 1447–1459.

Zhang Q, Magnusson MK, Mosher DF (1997). Lysophosphatidic acid and microtubule-destabilizing agents stimulate fibronectin matrix assembly through Rho-dependent actin stress fiber formation and cell contraction. Mol Biol Cell 8, 1415–1425.

Zhang R, Wang N, Zhang M, Zhang LN, Guo ZX, Luo XG, Zhou H, He HP, Zhang TC (2015). Rho/MRTF-A-induced integrin expression regulates angiogenesis in differentiated multipotent mesenchymal stem cells. Stem Cells Int 2015, 534758.